Thermal properties of (4) Vesta derived from Herschel measurements

C. Leyrat, A. Barucci, T. Mueller, L. O'rourke, I. Valtchanov, S. Fornasier

A&A 539, A154 (2012)
DOI: 10.1051/0004-6361/201117793

Astronomy & Astrophysics

Thermal properties of (4) Vesta derived from *Herschel* measurements

C. Leyrat[1], A. Barucci[1], T. Mueller[2], L. O'Rourke[3], I. Valtchanov[3], and S. Fornasier[1]

[1] LESIA, Observatoire de Paris, CNRS, UPMC, Université Paris-Diderot, 5 place Jules Janssen, 92195 Meudon, France
e-mail: cedric.leyrat@obspm.fr
[2] Max Planck Institute, MPE, Garching, Germany
[3] ESAC (European Space Astronomy Centre), PO Box 78, 28691 Villanueva de la Canada, Madrid, Spain

Received 29 July 2011 / Accepted 21 January 2012

ABSTRACT

Aims. We report in this paper the results provided by new infrared observations of the asteroid (4) Vesta obtained between April 2010 and June 2010 with the *Herschel* space observatory (ESA) in the wavelength range 70–500 μm when the asteroid was seen from the Northern hemisphere. Over this period, the thermal flux of Vesta was observed at different rotational phases and a large fraction of the surface was visible.

Methods. A thermophysical model was used to derive thermal properties such as infrared emissivity, thermal inertia and surface roughness.

Results. We found an average thermal inertia $\Gamma = 20^{+20}_{-10}$ J m^{-2} K^{-1}s$^{-1/2}$. The surface roughness on the Northern hemisphere, while poorly constrained, appears to be low on Vesta with a mean slope angle $\bar{\theta} \sim 23°$. Surface temperatures range from 40 K to 248 K. We cannot confirm any longitudinal variation of the thermal flux as it remains within the error bars. More observations are needed to confirm if the eastern hemisphere could have either a slightly higher thermal inertia suggesting a rockier surface or a smooth surface with a higher beaming factor. We emphasize an important decrease of the infrared emissivity of Vesta with the wavelength, ranging from 0.9 at 70 μm to 0.70 at 500 μm.

Key words. minor planets, asteroids: general – methods: data analysis – conduction – space vehicles: instruments

1. Introduction

The asteroid (4) Vesta is one of the most interesting small bodies of our solar system. Its semi-major axis is 2.361 AU, implying that Vesta is located in the inner asteroid main-belt. Disk-resolved *Hubble* space telescope (HST) observations have been used to estimate its shape (Thomas et al. 1997), giving an equivalent radius of about 258 ± 5 km. A huge crater located at the South pole was identified by Thomas et al. (1997), which was suggested to be most likely due to to an impact with a 35 km projectile (Asphaug 1997) occurred in the past. Vesta is large enough to be a differentiated body. Observations in visible wavelengths revealed mineralogic variations across its surface (Li et al. 2010) and have found that the eastern and western hemispheres show markedly different terrains respectively with high and low geometric visible albedos (up to 20% of a difference). This is suggestive of different surface compositions (Shestopalov et al. 2010) with the dark geological units being due to the presence of basalts.

Thermal observations in mid- and far-infrared have been used in the past to constrain surface properties of Vesta, both from ground as well as space based namely the NASA and ESA (European Space Agency) space observatories IRAS and ISO. Lebofsky et al. (1991) found a thermal inertia Γ = 40 J m^{-2} K^{-1} s$^{-1/2}$ comparable to that of the moon surface. Müller & Lagerros (1999) found a slightly lower value and emphasized a drop of the emissivity in the far-IR beyond 50 μm. Low emissivity (~0.6) was also found in millimeter and sub-millimeter wavelengths (Müller & Barnes 2007).

Because of the significant scientific interest in this asteroid, Vesta was chosen to be the first of the two asteroid targets to be visited by the DAWN mission (NASA). The spacecraft arrived at Vesta on 17 July 2011 with the intention to orbit the asteroid during one complete year. With the VIR spectro-imager onboard DAWN (de Sanctis et al. 2010) obtaining several spectral frames of the surface between 0.25 and 5 μm, these will be very useful to determine the surface compositions and temperatures. The variations of the thermal emission with the local time allow Γ to be determined, which gives important clues on the surface porosity, allowing to distinguish between rocky and dusty surfaces with good spatial resolution (Sykes et al. 2010). Macroscopic surface roughness can also be constrained from thermal infrared data. The measurements presented in this paper are considered an important data set to complement what will be produced and analyzed with VIR spectro-imager.

In this paper, we report new infrared observations of Vesta, at a variety of phase angles, performed between 70 to 500 μm with the *Herschel*[1] space observatory between April and June 2010. These *Herschel* disk-unresolved data sets allow the average thermal inertia, rugosity and emissivity to be determined, while DAWN will provide physical quantities at shorter wavelengths and with better spatial resolution.

[1] *Herschel* is an ESA space observatory with science instruments provided by European-led Principal Investigator consortia and with important participation from NASA.

2. *Herschel* observations and data reduction

The ESA *Herschel* space observatory was launched in 2009 and is now orbiting around the 2nd Earth Lagrangian point (L2) at 1.5 Million km from Earth. It has three science instruments onboard covering the far-infrared part of the spectrum, two of which, PACS (Photodetector Array Camera and Spectrometer) and SPIRE (Spectral and Photometric Imaging REceiver), have been used to observe the thermal emission of Vesta. They work respectively in the wavelength range 60–210 μm and 250–500 μm. Several high quality observations of Vesta were obtained as part of calibration campaigns for the two instruments. We analyzed the photometric data taken with PACS in April 2010 and with SPIRE in May and June 2010 to determine the thermal properties of the asteroid.

2.1. PACS data reduction

Vesta has been observed 16 times with PACS, at three wavelengths (70, 100 and 160 μm), between 24 April 2010 and 27 April 2010. The PACS measurements were taken in two different modes: mini scan-map and chop-nod, and were processed using HIPE 5.0. We refer the reader to Poglitsch et al. (2010) for more details about the method. The observed flux were aperture and color corrected[2] to obtain monochromatic flux densities at the PACS bolometer reference wavelengths of 70.0, 100.0 and 160.0 μm. This correction consists of dividing the flux by a factor which is provided on Table 3 on Poglitsch et al. (2010). For Vesta, this factor is chosen as 0.986 at 70 μm, 1.03 at 100 μm and 1.07 at 160 μm. The signal to noise ratio is higher than 1000 and the errors are determined by the absolute uncertainty of the PACS system. A correction for the systematic differences between the two different observing techniques (4–6%) has been done. The final fluxes obtained for the PACS instrument data sets were deemed to be accurate within 5% based upon the latest calibrations existing. All the PACS measurements fluxes are described in Table 1.

For each observation, the associated geometrical parameters were computed using the IMCCE ephemeris server[3]. In April 2010, the northern hemisphere was tilted toward *Herschel* with the morning side of Vesta was visible from *Herschel* (see Table 1).

2.2. SPIRE measurements

Vesta was also observed by SPIRE at 250, 350 and 500 μm in a small scan map mode. Observations took place on six occasions between May 3, 2010 and June 28, 2010, at different aspect angles. The data has been processed using the *Herschel* interactive processing environment (HIPE, version 6.1) after which correction for the objects movement during the observation was applied to the data. Data were processed using the standard timeline fitter with the output fluxes then color corrected according to the values defined in the SPIRE observers' manual, Sect. 5.2.8[4]. This correction is necessary because the SPIRE photometry calibration assumes a constant spectral slope S_ν in band, while a blackbody spectrum in the Rayleigh-Jeans regime has a different spectral shape, i.e. $S_\nu \sim \nu^2$.

The SPIRE photometer flux calibration is based on observations of Neptune (see the SPIRE observers' manual for more details). The final flux density errors include a 7% conservative flux uncertainty from the Neptune model, in addition to the fitted peak error. Measurements and geometries are also described in Table 1.

3. Analysis of thermal data

3.1. Shape and Thermal model

To derive thermal properties of Vesta, we used the Thomas et al. (1997) shape model composed of 5120 facets and 2562 vertices, and we combined this shape model with a thermophysical model (TPM) that is fully described in Leyrat et al. (2011). This TPM can predict the asteroid surface temperature at different epochs. The local illumination conditions (incidence angle and shadows) of each facet are computed over one complete daily rotation using the given shape and the orientation with respect to the Sun. The pole solution is given by Archinal et al. (2011) and is very similar to the one found by Thomas et al. (1997). The thermal response of the surface is then computed assuming a 1-D heat conduction into the sub-surface. The model predicts the surface temperature at a given local time and with an assumed set of thermal parameters. It then produces thermal infrared spectra when the asteroid is seen from a specific point of view. Small scale surface roughness is described by the self-heating parameter ξ (Lagerros 1997), and used by Davidsson et al. (2009). Its physical meaning differs from the classical beaming parameter η with the mathematical formalism being the same. Davidsson et al. (2009) have shown that when self heating is dominated by thermal emission rather than scattered light, the classical beaming parameter η is equivalent to $1 - \xi\epsilon$, where ϵ is the IR emissivity.

The bolometric infrared emissivity is first fixed to 0.9, the value usually cited in the literature for asteroids. Its variations with wavelengths are described later. The Bond albedo A_B, which controls the total flux absorbed by a surface, depends on the geometric visible albedo p_V and the phase integral q by the relation $A_P = p_V q$. In accordance with Bowell et al. (1989), q is derived from the slope parameter G of HG-photometric system via the equation $q = 0.290 + 0.684$ G. Recent observations of Vesta obtained by the OSIRIS/Rosetta cameras (ESA) have been used to derive $G = 0.27$, and an average value of the visual geometric albedo $p_V = 0.34$ at 535 nm (Fornasier et al. 2011). This implies that $q = 0.47$.

The average Bond albedo is then fixed to $A_B = 0.16$. However, disk-resolved images obtained with the HST have revealed that Vesta shows variations of the albedo over its surface (Binzel et al. 1996; Li et al. 2010). Those observations indicate a higher albedo in the Eastern hemisphere than in the Western side. The observed visible light curves depends not only on the apparent variations of the cross section of one rotation, but also on the modulations of the albedo. While small variations of the surface albedo may not affect significantly the surface temperature T (the latter being proportional to $(1 - A_B)^{1/4}$), we have included in our model the spatial distribution of the albedo, leaving the thermal inertia, the surface roughness and the emissivity as a potential explanation for variations in thermal radiations from Vesta. A_B was computed for each facet of the shape model by projecting the visual albedo map (p_v) obtained at wavelength $\lambda = 673$ nm from Li et al. (2010) for latitudes ranging from −60 to +20 degrees and from Binzel et al. (1996) up to +60 deg

[2] See http://herschel.esac.esa.int/twiki/pub/Public/PacsCalibrationWeb/pacs_bolo_fluxcal_report_v1.pdf for more details about the factor corrections.

[3] http://www.imcce.fr

[4] Available from the *Herschel* Science Centre, http://herschel.esac.esa.int/Docs/SPIRE/pdf/spire_om.pdf

Table 1. PACS and SPIRE observations with geometrical parameters obtained with the IMCCE ephemeris site.

Time (UTC)	λ (μm)	Flux (Jy)	σ flux (Jy)	Phase (deg)	Obs long	Obs lat	Sun long	Sun lat	r	Δ
				PACS						
2010-04-24T00:12:41	70.0	203.982	6.756	24.4	54.82	23.63	81.13	23.41	2.331	1.804
2010-04-24T00:38:13	70.0	197.399	6.538	24.4	26.75	23.63	53.06	23.41	2.331	1.805
2010-04-27T03:09:14	70.0	188.975	6.259	24.8	45.92	23.75	72.68	23.19	2.328	1.837
2010-04-24T01:05:01	100.0	107.596	2.959	24.4	356.42	23.64	22.74	23.41	2.331	1.805
2010-04-24T01:30:33	100.0	108.405	2.981	24.4	328.35	23.64	354.67	23.41	2.331	1.805
2010-04-27T03:24:17	100.0	100.466	2.763	24.8	29.08	23.75	55.84	23.19	2.328	1.837
2010-04-24T00:12:41	160.0	44.044	1.828	24.4	54.82	23.63	81.13	23.41	2.331	1.804
2010-04-24T00:38:13	160.0	43.694	1.813	24.4	26.75	23.63	53.06	23.41	2.331	1.804
2010-04-24T01:05:01	160.0	43.760	1.816	24.4	356.42	23.64	22.74	23.41	2.331	1.805
2010-04-24T01:30:33	160.0	44.567	1.850	24.4	328.35	23.64	354.67	23.41	2.331	1.805
2010-04-27T03:09:14	160.0	40.428	1.678	24.8	45.92	23.75	72.68	23.19	2.328	1.837
2010-04-27T03:24:17	160.0	40.037	1.662	24.8	27.95	23.75	54.71	23.19	2.328	1.837
2010-04-27T03:05:29	70.0	183.198	6.073	24.8	50.41	23.75	77.17	23.19	2.328	1.837
2010-04-27T03:05:29	160.0	42.436	1.798	24.8	50.41	23.75	77.17	23.19	2.328	1.837
2010-04-27T03:20:32	100.0	100.360	2.768	24.8	33.57	23.75	60.33	23.19	2.328	1.837
2010-04-27T03:20:32	160.0	42.142	1.774	24.8	33.57	23.75	60.33	23.19	2.328	1.837
				SPIRE						
2010-06-28T20:26:03	250	9.50	0.66	24.3	153.09	24.31	177.69	17.43	2.267	2.503
2010-06-28T20:26:03	350	4.63	0.32	24.3	153.09	24.31	177.69	17.43	2.267	2.503
2010-06-28T20:26:03	500	2.26	0.16	24.3	153.09	24.31	177.69	17.43	2.267	2.503
2010-06-19T15:52:37	250	10.51	0.74	25.1	277.90	24.59	303.78	18.41	2.276	2.412
2010-06-19T15:52:37	350	5.20	0.36	25.1	277.90	24.59	303.78	18.41	2.276	2.412
2010-06-19T15:52:37	500	2.50	0.17	25.1	277.90	24.59	303.78	18.41	2.276	2.412
2010-06-10T16:50:16	250	11.42	0.8	25.8	5.43	24.71	32.32	19.32	2.285	2.321
2010-06-10T16:50:16	350	5.57	0.39	25.8	5.43	24.71	32.32	19.32	2.285	2.321
2010-06-10T16:50:16	500	2.70	0.19	25.8	5.43	24.71	32.32	19.32	2.285	2.321
2010-05-30T15:11:51	250	12.24	0.86	26.3	261.00	24.67	288.75	20.39	2.295	2.203
2010-05-30T15:11:51	350	6.07	0.42	26.3	261.00	24.67	288.75	20.39	2.295	2.203
2010-05-30T15:11:51	500	2.99	0.21	26.3	261.00	24.67	288.75	20.39	2.295	2.203
2010-05-18T14:24:01	250	14.03	0.98	26.3	277.84	24.44	305.95	21.47	2.307	2.071
2010-05-18T14:24:01	350	6.76	0.47	26.3	277.84	24.44	305.95	21.47	2.307	2.071
2010-05-18T14:24:01	500	3.31	0.23	26.3	277.84	24.44	305.95	21.47	2.307	2.071
2010-05-03T10:29:07	250	16.60	1.16	25.5	316.47	23.97	343.92	22.71	2.322	1.905
2010-05-03T10:29:07	350	8.17	0.57	25.5	316.47	23.97	343.92	22.71	2.322	1.905
2010-05-03T10:29:07	500	4.00	0.28	25.5	316.47	23.97	343.92	22.71	2.322	1.905

Notes. λ is the wavelength, *Phase* is the solar phase angle in degrees, *Obs long* and *Sun long* are the planetocentric sub-observer and sub-solar longitudes in Vesta's reference frame, *Obs lat* and *Sun lat* are the planetocentric sub-observer and sub-solar latitudes in Vesta's reference frame, r is the heliocentric distance, Δ is the *Herschel*-Vesta distance. Fluxes have been color corrected (see text for more details).

of latitudes. The upper panel in Fig. 1 shows the corresponding surface A_B map, ranging from 0.14 to 0.19. The Bond albedo associated to facets located at high latitudes (greater than 60 deg and lower than −60 deg) is fixed to 0.16, i.e. the average value. We checked that the distribution of the surface albedo variations p_v is consistent with visual light curves obtained previously at similar geometry and phase angles (Taylor et al. 1976). The disk-integrated bond albedo $A_{B\,Disk}$ is shown versus the longitude in Fig. 1 (lower panel) and obtained by normalizing the average value of A_B to the apparent cross section Ω of Vesta.

The disk-integrated model flux at the wavelength λ is then given by

$$F_\lambda = \frac{1}{\pi\Delta^2}\int (1-\xi\epsilon)\epsilon B_\lambda(T)\cos(\theta)\mathrm{d}S, \quad (1)$$

where Δ is the distance to *Herschel*, B_λ the Planck function at temperature T and $\cos(\theta)\mathrm{d}S$ the projected area of the surface element $\mathrm{d}S$. The free parameters are the thermal inertia Γ which describe the thermal response of the surface, and ξ. Γ depends on the thermal conductivity K, the heat capacity C and the volume density ρ as follows $\Gamma = \sqrt{K\rho C}$.

3.2. Thermal properties of Vesta with Herschel data

A TPM χ^2 test was run using a range of thermal inertias (from 1 to 70 J m^{-2} K^{-1} s$^{-1/2}$) and a range of ξ from 0.02 to 0.45 with the goal to find the best fit obtained with specific Γ-ξ couple values when comparing the observations/TPM ratio with wavelength, rotational phase and aspect angle. We first fitted the TPM to the whole data set. The best fit was obtained for $\Gamma = 20^{+20}_{-10}$ J m^{-2} K^{-2} s$^{-1/2}$ and $\xi = 0.15^{+0.10}_{-0.13}$. While poorly constrained because of the wavelength range that corresponds to the Rayleigh-Jeans regime, this low thermal inertia is in good agreement with previous estimations (Mueller & Lagerros 1998), and is typical of large main belt asteroids. It implies a surface covered by a thick regolith layer that decreases the efficiency of the thermal conduction over the first millimeters, because of the porosity.

Using the Lagerros (1998) TPM, Mueller & Lagerros (1998) found very high crater densities that can increase significantly the surface temperature (especially when the local incidence angle is important) because of self-heating inside the craters. According to Davidsson et al. (2009), in the case of a Gaussian distribution of the surfaces local slopes, the ξ parameter can be

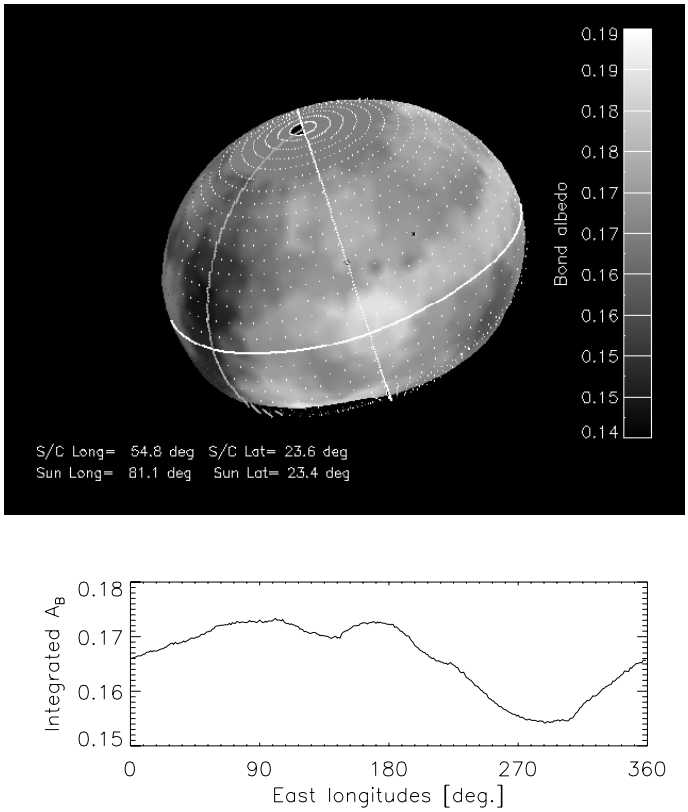

Fig. 1. *Top*: Bond albedo variations obtained from Binzel et al. (1996) and Li et al. (2010) as seen on April 24, 2010 at 00h12 UT. The solid meridians represent the zero longitude and the sub-observer meridian. *Bottom*: disk integrated Bond albedo during one complete rotation computed for April 24, 2010.

directly linked to the mean slope angles $\bar{\theta}$ of the surface as described by Hapke (1984):

$$\xi = 1 - \frac{E_1(\cot^2\bar{\theta}/\pi)}{\pi \tan\bar{\theta}\,\mathrm{erfc}(\cot\bar{\theta}/\sqrt{\pi})} \quad (2)$$

where $E_1(x) = \int_1^\infty \mathrm{e}^{-xt}/t\mathrm{d}t$ is the first order exponential integral (with $x = \cot^2\bar{\theta}/\pi$), and erfc is the complementary error function. Our value of $\xi = 0.15$ corresponds to $\bar{\theta} \sim 23°$. This value is similar to that reported for typical lunar materials or for most asteroids and comets, but slightly smaller to that already found for some small bodies (5535 Annefrank, Hillier et al. 2011; 1 Ceres, Li et al. 2006). This suggests a low degree of surface roughness on Vesta (at least from the observed latitudes (i.e. from −65 to +90 deg)) and a rockier-smooth surface. Interestingly, Chamberlain et al. (2011) found similar results on the Southern hemisphere which is now observed by Dawn.

We looked for potential longitudinal variations of the mid infrared and submillimeter flux behavior. The lack of multi-wavelength data covering a full rotational phase prevented us from constraining accurately both ξ and Γ for each of Vesta's hemispheres separately. Figure 2 shows how the ratio between the measured flux and the TPM predictions (so called $F_{\rm obs}/F_{\rm TPM}$) varies with the planetocentric longitudes. The plotted $F_{\rm obs}/F_{\rm TPM}$ is corrected from the global derived wavelength dependent emissivity as detailed in the following section. Potential variations can be associated to variations of the

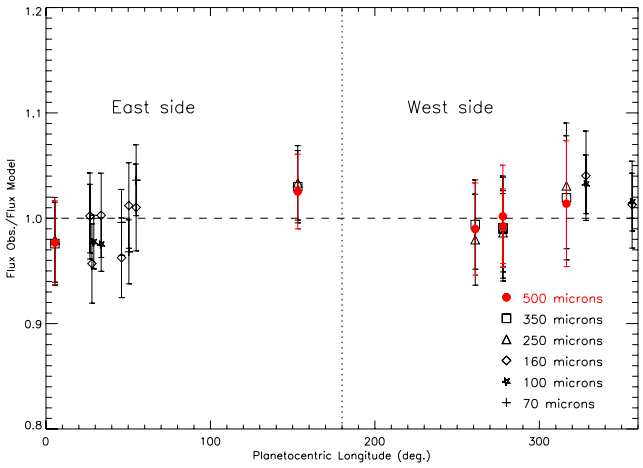

Fig. 2. PACS and SPIRE observations of Vesta divided by the corresponding best-fit TPM predictions as function of the sub-observer planetocentric longitudes. This ratio has been corrected from the wavelength emissivity dependance. Longitudes increase eastwards. SPIRE observations performed at 500 μm are plotted in red to help the reader to compare data at different longitudes.

roughness, the local emissivity or the thermal inertia, as the effect of the albedo variegation has already been included in our model.

Since the radiated thermal intensity varies as T^4 at the first order, the effect of infrared beaming is actually to cool the mean temperature of the surface. Thus, infrared beaming increases $F_{\rm obs}/F_{\rm TPM}$ at short infrared wavelengths but decreases it when infrared flux is approximated by the Rayleigh-Jeans law at submillimeter wavelengths (Redman et al. 1998), which is the case for SPIRE data.

We observed a very weak increase of observed flux from 250 to 500 μm on the eastern hemisphere (especially around 150 degrees longitudes), but we cannot conclude that this behavior is associated to variations of the surface properties as the amplitude variations remains within the 1-σ error bars (Fig. 2). Potential increase of $F_{\rm obs}/F_{\rm TPM}$ would have suggested a lower surface temperature that could have been explained either by a local decrease of ξ (i.e. an increase of the beaming factor η) or a higher thermal inertia (as Vesta is observed from low phase angle). If the observed anomaly would have been confirmed around 150 deg longitudes, it would have implied that the surface of Vesta on this area on the Northern hemisphere would have been smoother or rockier than the other parts of the asteroid. Interestingly, Chamberlain et al. (2011) already found a similar and much more pronounced behavior in the Southern latitudes with a classical STM thermal model. A similar result on the northern hemisphere still has to be confirmed by Dawn or by mid-infrared observations.

3.3. Emissivity

The wavelength dependent emissivity $\epsilon_{\rm IR}(\lambda)$ is determined in a second step by comparing the observed flux to the TPM output that best fit the data. Figure 3 shows the ratio between the observed flux and the output of our TPM, as a function of wavelength. At short wavelengths (i.e. $\lambda \leq 100$ μm), $\epsilon_{\rm IR}$ is slightly larger than 0.9, the value applicable for most asteroids. A clear trend of decreasing emissivity $\epsilon_{\rm IR}(\lambda)$ can be seen for $\lambda \geq 100\,\mu$m, reaching ~0.75–0.80 at 500 μm. While such a cut-off was not

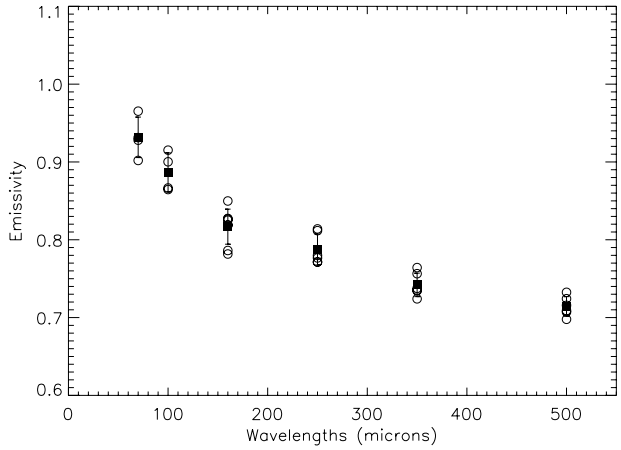

Fig. 3. Emissivity as a function of wavelength. Circles represent all data (over the whole Vesta surface) while filled squares are the average value for each wavelength.

considered significant in previous studies at wavelengths below ~200 μm (Hormuth & Müller 2009), Müller (2002) emphasized a systematic drop of the emissivity with the ISO data beyond 150 μm.

This global $\epsilon_{IR}(\lambda)$ behavior observed with *Herschel* confirms previous studies obtained by Redman et al. (1998) in submillimeter wavelengths and by Müller & Barnes (2007) and Mueller & Lagerros (1998) in millimeter wavelengths. Redman et al. (1992) calculated a lower Rayleigh-Jeans temperature at submillimeter wavelengths compared to the mid-IR. They suggested that this important decrease of $\epsilon_{IR}(\lambda)$ with wavelength is an indication for the presence of a dusty and porous regolith. Indeed, scattering processes by grains smaller than 100 μm within the regolith can reduce the emissivity in a wavelength dependent fashion (Redman et al. 1992).

4. Surface temperatures of Vesta

Based upon the temperatures predictions provided by the thermophysical model and the surface roughness assumptions, we looked at the modelled temperature distribution at the surface of Vesta. From the TPM facets temperatures distribution, we found a minimum temperature of ~40 K and a peak temperature of 248 K. The maximum temperature is slightly shifted from the sub-solar point towards the East by 15–20 degrees in longitude due to the non-zero thermal inertia (Fig. 4). While the upper temperatures are highly constrained, considering that *Herschel* has mainly observed the day side of Vesta and also because of the high quality of the PACS and SPIRE data, the lower ones are less constrained due to the observing geometries that are related only to the day side of the surface. The south pole temperatures are also poorly constrained as our latitude coverage is limited to [−65, +90] degrees and also because this area is not illuminated by the Sun during our observations. Our TPM takes into account only the diurnal thermal cycle and does not include any seasonal effect. Thus, emission of the thermal waves at the South pole, that comes from the deep layers heated during the northern winter, are not computed and we cannot explain a non-zero surface temperature using our thermal model.

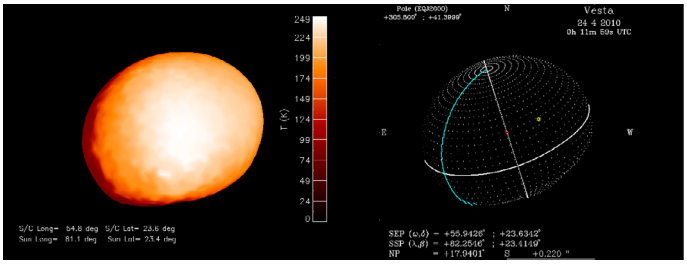

Fig. 4. *Left*: temperature distribution on the surface of (4) Vesta on 2010-Apr.-24 00:12:00 UT, based on the HST-shape model in combination with the TPM. The morning side is on the left. *Right*: topographic coordinate system produced with the IMCCE ephemeris at the same epoch. Blue line represents the central longitude, and circles indicates the sub-solar and sub-observer points.

5. Conclusions

The Northern hemisphere of (4) Vesta has been observed in the far-infrared with *Herschel*'s SPIRE and PACS instruments. Using a thermophysical model, thermal properties of the asteroid have been constrained. The derived average thermal inertia ($\Gamma = 20^{+20}_{-10}$ J m^{-2} K^{-2} s$^{-1/2}$) is in good agreement with previous estimations (Mueller & Lagerros 1998) and suggests the presence of fine regolith at the surface. As we do not have systematic measurements covering the full rotational curve of Vesta, it is difficult to check whether or not thermal properties vary across the surface. A very weak behavior could suggest variations of thermal properties with longitudes, but they remain within the error bars. Such a result will have to be confirmed by DAWN.

The surface temperatures on the observed latitudes (i.e. from −65 to +90 degrees) vary from almost 40 to 248 K, the maximum being slightly lower than the estimated sub-solar temperature (252 K) when $\Gamma = 0$ J m^{-2} K^{-2} s$^{-1/2}$ is assumed. While local topography may add some mutual heating and thus affect the estimated maximum surface temperature, the lowest temperatures close to the South pole cannot be constrained properly by our TPM.

We also emphasize a strong dependence of the emissivity with wavelengths in the far-IR, towards 100 μm, that can be explained by scattering processes of infrared photons in the regolith. At the considered wavelengths, *Herschel* measurements correspond to the sub-surface layers. VIR/DAWN data will soon perform near-IR in-situ measurements of the Northern latitudes and the instrument is expected to provide updated constraints on the thermal inertia and surface roughness. This combination of mid-IR data from VIR/Dawn with the *Herschel* far-IR disk-integrated data will be an important and significant contribution in increasing our knowledge on the physical processes that drive the surface of Vesta.

Acknowledgements. We thank the anonymous reviewer for the comments and suggestions received, which improved the quality of this work.

References

Archinal, B. A., A'Hearn, M. F., Bowell, E., et al. 2011, Cel. Mech. Dyn. Astron., 109, 101
Asphaug, E. 1997, Meteor. Planet. Sci., 32, 965
Binzel, R. P., Gaffey, M. J., Thomas, P. C., et al. 1996, in Evolution of Igneous Asteroids: Focus on Vesta and the HED Meterorites, ed. D. W. Mittlefehldt, & J. J. Papike, 2
Bowell, E., Hapke, B., Domingue, D., et al. 1989, in Asteroids II, ed. R. P. Binzel, T. Gehrels, & M. S. Matthews, 524
Chamberlain, M. A., Sykes, M. V., & Tedesco, E. F. 2011, Icarus, 215, 57

Davidsson, B. J. R., Gutiérrez, P. J., & Rickman, H. 2009, Icarus, 201, 335
de Sanctis, M. C., Coradini, A., Ammannito, E., et al. 2010, Space Sci. Rev., 103
Fornasier, S., Mottola, S., Barucci, M. A., Sierks, H., & Hviid, S. 2011, A&A, 533, L9
Hapke, B. 1984, Icarus, 59, 41
Hillier, J. K., Bauer, J. M., & Buratti, B. J. 2011, Icarus, 211, 546
Hormuth, F., & Müller, T. G. 2009, A&A, 497, 983
Lagerros, J. S. V. 1997, A&A, 325, 1226
Lagerros, J. S. V. 1998, A&A, 332, 1123
Lebofsky, L. A., Hubbard, W. B., Asphaug, E., et al. 1991, in Lunar and Planetary Inst. Technical Report, Lunar and Planetary Institute Science Conference Abstracts, 22, 793
Leyrat, C., Coradini, A., Erard, S., et al. 2011, A&A, 531, A168
Li, J.-Y., McFadden, L. A., Parker, J. W., et al. 2006, in 36th COSPAR Scientific Assembly, 36, 1078
Li, J.-Y., McFadden, L. A., Thomas, P. C., et al. 2010, Icarus, 208, 238
Mueller, T. G. & Lagerros, J. S. V. 1998, A&A, 338, 340
Müller, T. G. 2002, Meteor. Planet. Sci., 37, 1919
Müller, T. G. & Barnes, P. J. 2007, A&A, 467, 737
Müller, T. G. & Lagerros, J. S. V. 1999, BAAS, 31, 1075
Poglitsch, A., Waelkens, C., Geis, N., et al. 2010, A&A, 518, L2
Redman, R. O., Feldman, P. A., Matthews, H. E., Halliday, I., & Creutzberg, F. 1992, AJ, 104, 405
Redman, R. O., Feldman, P. A., & Matthews, H. E. 1998, ApJ, 116, 1478
Shestopalov, D. I., McFadden, L. A., Golubeva, L. F., & Orujova, L. O. 2010, Icarus, 209, 575
Sykes, M. V., Tricarico, P., & Li, J. 2010, in BAAS, AAS/Division for Planetary Sciences Meeting Abstracts #42, 42, 1033
Taylor, R. C., Gehrels, T., & Capen, R. C. 1976, AJ, 81, 778
Thomas, P. C., Binzel, R. P., Gaffey, M. J., et al. 1997, Icarus, 128, 88